JACS
JOURNAL OF THE AMERICAN CHEMICAL SOCIETY
Article
Cite This: J. Am. Chem. Soc. 2019, 141, 16323−16330
pubs.acs.org/JACS

Room Temperature Metallic Conductivity in a Metal−Organic Framework Induced by Oxidation

Andrew J. Clough,[†] Nicholas M. Orchanian,[†] Jonathan M. Skelton,[‡] Abbey J. Neer,[†] Sebastian A. Howard,[§] Courtney A. Downes,[†] Louis F. J. Piper,[§,∥] Aron Walsh,[⊥,#] Brent C. Melot,*[,†] and Smaranda C. Marinescu*[,†]

[†]Department of Chemistry, University of Southern California, Los Angeles, California 90089, United States
[‡]School of Chemistry, University of Manchester, Manchester M13 9PL, United Kingdom
[§]Department of Physics, Applied Physics and Astronomy, Binghamton University, Binghamton, New York 13902, United States
[∥]Materials Science & Engineering, Binghamton University, Binghamton, New York 13902, United States
[⊥]Department of Materials, Imperial College London, London SW7 2AZ, United Kingdom
[#]Department of Materials Science and Engineering, Yonsei University, Seoul 03722, Korea

Supporting Information

ABSTRACT: Metal−organic frameworks (MOFs) containing redox active linkers have led to hybrid compounds exhibiting high electrical conductivity, which enables their use in applications in electronics and electrocatalysis. While many computational studies predict two-dimensional (2D) MOFs to be metallic, the majority of experiments show decreasing conductivity on cooling, indicative of a gap in the electronic band structure. To date, only a handful of MOFs have been reported that exhibit increased electrical conductivity upon cooling indicative of a metallic character, which highlights the need for a better understanding of the origin of the conductivity. A 2D MOF containing iron bis(dithiolene) motifs was recently reported to exhibit semiconducting behavior with record carrier mobility. Herein, we report that high crystallinity and the elimination of guest species results in an iron 2,3,6,7,10,11-tripheylene-hexathiolate (THT) MOF, FeTHT, exhibiting a complex transition from semiconducting to metallic upon cooling, similar to what was shown for the analogous CoTHT. Remarkably, exposing the FeTHT to air significantly influences the semiconducting-to-metallic transition temperature (100 to 300 K) and ultimately results in a material showing metallic-like character at, and above, room temperature. This study indicates these materials can tolerate a substantial degree of doping that ultimately results in charge delocalization and metallic-like conductivity, an important step toward enabling their use in chemiresistive sensing and optoelectronics.

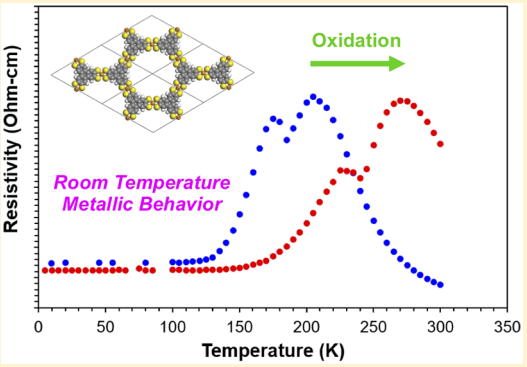

INTRODUCTION

Metal−organic frameworks (MOFs) are crystalline nanoporous materials composed of metal ions or clusters linked by organic ligands.[1−4] The hybrid organic/inorganic nature of MOFs allows for synthetic tunability, leading to MOFs with varying pore sizes and chemical environments and, therefore, different physical and chemical properties.[1−5] These properties have led to applications primarily in gas storage and separation[6−8] and catalysis,[9] which take advantage of the inherent porosity and high surface area of these materials.[10] The use of MOFs in technologies that require charge transport, such as electronics[11,12] and electrocatalysis,[13] has lagged due to their generally poor electrical conductivity. The weak covalent overlap between the metal and ligand orbitals results in localized (small bandwidth) electronic band structures with low mobility charge carriers, preventing fast charge transport through the framework. This leads to materials with insulating or large gap semiconducting behavior.[5,14,15] Efforts to reduce the barriers to charge transport have included the addition of guest species,[16−18] doping,[19−21] and variation of the metal center and its oxidation state.[22−26] These modifications can encourage through-space[27,28] or through-bond[29] electronic transport and have led to MOFs with improved conductivities, with one example reporting tunable conductivity over 6 orders of magnitude.[17]

Recently, the development of MOFs with redox active linkers has led to a breakthrough in the field of electrically conductive MOFs.[11,12,15,30−34] Several two- and three-dimensional (2D/3D) frameworks with planar, π-conjugated, and redox-active linkers, like semiquinones/cathecolates,[35−43] diimines,[44−48] and dithiolenes,[19,21,48−61] have been reported

Received: June 28, 2019
Published: September 25, 2019

DOI: 10.1021/jacs.9b06898
J. Am. Chem. Soc. 2019, 141, 16323−16330

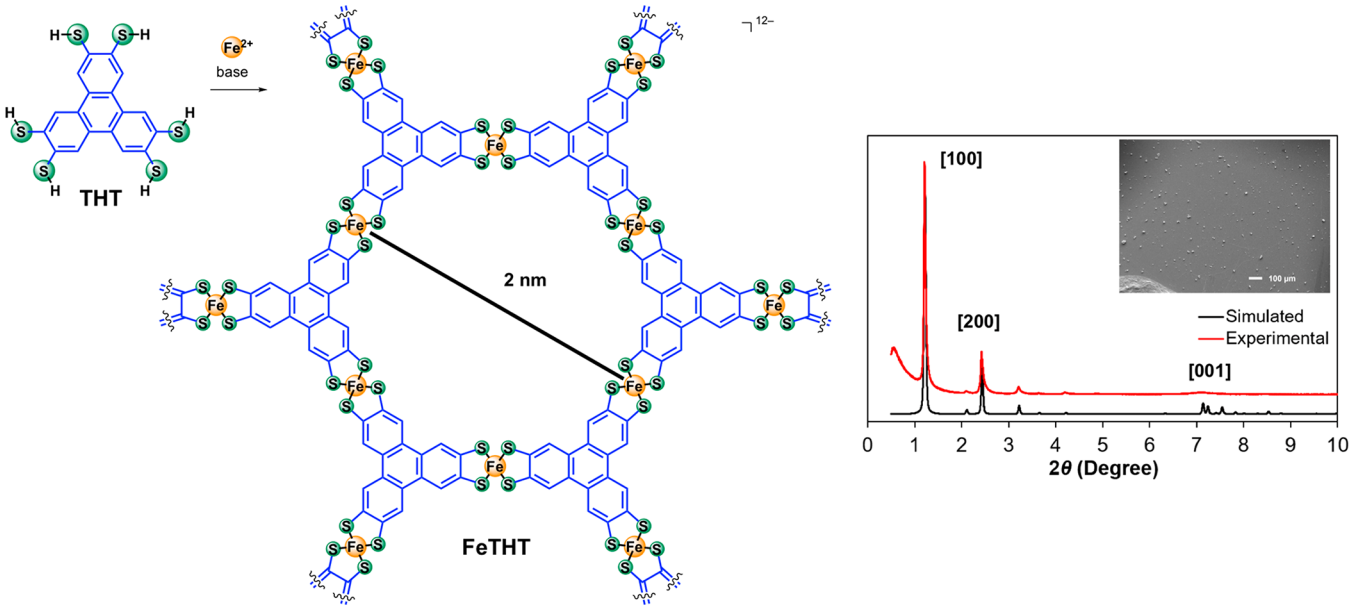

Figure 1. Synthesis and structure of the **FeTHT** framework. The plot shows a comparison of the experimental (red; synchrotron radiation with λ = 0.414576 Å) and simulated (black) PXRD patterns, and the inset shows an SEM image at 75× low magnification.

to display high electrical conductivity. Yet, while computational studies often predict these 2D MOFs to be metallic,[50,62−65] the majority of the frameworks reported display a decrease in conductivity on cooling as thermally populated carriers are lost. In contrast, the primary mechanism for carrier scattering in metals is due to lattice vibrations that are significantly dampened at lower temperatures, resulting in more efficient transport on cooling. We previously reported the temperature-dependent electrical conductivity of a 2D cobalt 2,3,6,7,10,11-tripheylenehexathiolate (THT) MOF.[52] While the measured conductivity at 300 K was modest (3.2×10^{-2} S/cm), a complex transition from semiconducting to metallic behavior was observed on cooling. This represented the first direct experimental observation of a MOF exhibiting metallic conductivity. The metallic character was corroborated by density-functional theory (DFT) calculations, which predicted semimetallic behavior through electronic states arising from interlayer overlap of metal d and ligand p orbitals. This complex behavior was attributed to a convolution of thermal expansion along the *c*-direction, stacking faults leading to misalignment of the layers, and significantly different transport at the grain-boundaries.

Recently, an analogous iron THT MOF with ammonium charge-compensating cations, $Fe_3(THT)_2(NH_4)_3$, was studied using high-frequency terahertz photoconductivity and Hall effect measurements. The reported $Fe_3(THT)_2(NH_4)_3$ material displays semiconducting behavior with record room-temperature carrier mobilities.[55] The calculated band structure, which explicitly included ammonium counterions, predicts semiconducting behavior with a bandgap of ∼350 meV. Strong orbital hybridization is observed between the d orbitals of Fe, the bis(dithiolene) moieties, and the triphenylene units. While promising room-temperature mobilities were reported for this material, the reported temperature-dependent resistivity studies indicate a decrease in conductivity on cooling, in contrast to the cobalt analogue.[51] This discrepancy emphasizes the current knowledge gap in understanding the nature of charge transport in MOFs. This shortcoming is especially noteworthy in materials reported to date using benzenehexathiolate and hexaiminobenzene linkers, which display decreases in their conductivity on cooling, despite ultraviolet photoelectron spectroscopy (UPS) studies revealing Fermi edges that strongly suggest metallic character.[46,50,58]

Related studies of a copper benzenehexathiolate (CuBHT) MOF report a decrease in conductivity on cooling, consistent with semiconducting behavior.[49] Using a modified synthetic procedure, the crystallinity of the resulting CuBHT was improved as evidenced by powder X-ray diffraction (PXRD) studies.[61] Temperature-dependent resistivity studies of the crystalline MOF indicate a decrease in resistivity upon cooling, as expected for a metal, followed by the noteworthy observation of a superconducting transition at low temperatures.[61] These studies highlight the influence of crystallinity in dictating the transport properties of 2D MOFs (semiconducting vs metallic). Yet, ideally, the transition from semiconducting to metallic behavior would be controllable through chemical and postsynthetic modification rather than a reliance on single-crystal growth, which remains a substantial challenge in the field. As a promising example of this goal, the chemical reduction of an analogous silver benzenehexathiolate (AgBHT) 2D MOF was shown by UPS studies to eliminate the Fermi edge of the pristine material, suggesting a metallic-to-semiconducting transition, with a corresponding reduction (∼3500-fold) in the electrical conductivity.[58]

Motivated by the knowledge that metal identity, doping, and the presence of guest species all have significant influence on the electronic properties of metal bis(dithiolene) species and related 2D MOFs,[66−68] we present a modified synthetic procedure to prepare the **FeTHT** framework as a comparative analogue to **CoTHT**. This modified protocol is informed by DFT predictions and seeks to circumvent the inclusion of ammonium guest species and generate materials with improved crystallinity as a means of inducing the semiconducting-to-metallic transition observed in **CoTHT**. Temperature-dependent resistivity studies of the as-prepared **FeTHT** framework confirm a transition from semiconducting to metallic upon cooling, which is analogous to the behavior observed for the **CoTHT** system.[52] We further explore the

DOI: 10.1021/jacs.9b06898
J. Am. Chem. Soc. 2019, 141, 16323−16330

effect that exposure to oxygen has on the conductivity of the framework and show that oxidation of the sample leads to an increase in the semiconducting-to-metallic transition temperature as a function of exposure, resulting in a material with metallic-like character at room temperature. Using a combination of X-ray photoelectron spectroscopy (XPS) and magnetic studies, we confirm that both the metal center and the ligand scaffold in **FeTHT** are oxidized. These results show that the semiconducting-to-metallic transition temperature is highly sensitive to dopant concentrations and suggests that the development of controlled postsynthetic redox treatments could be effective at enhancing the functional properties of this family of materials.

RESULTS AND DISCUSSION

Synthesis and Characterization. The 2D **FeTHT** MOF was synthesized using a liquid−liquid interfacial reaction as previously reported for the cobalt analogue (Figure 1).[52,69] The trinucleating ligand scaffold, triphenylene-2,3,6,7,10,11-hexathiol, was treated with *N*-methyl-2-pyrrolidone (NMP) in an ethyl acetate solution and sonicated. The generated suspension was gently layered onto an aqueous solution of the Fe(II) chloride, leading to the formation of a black film of **FeTHT** at the liquid−liquid interface over the course of 5 days. The black film was then deposited onto glass substrates as thin films or collected as a powder for bulk measurements. This synthetic methodology is in contrast to that reported recently for $Fe_3(THT)_2(NH_4)_3$, where a solution of $Fe(acac)_2$ in chloroform was layered with an aqueous solution of THT ligand with NH_4OH as base.[55] Since our synthetic procedure does not include NH_4OH, the variations employed here serve to exclude the NH_4^+ guest species. This approach provides a platform for demonstrating the influence of guest species on bulk transport properties of the Fe system, as well as appropriately comparing the electronic behavior of the Fe and Co systems.

The crystallinity of the **FeTHT** framework was confirmed by PXRD using synchrotron radiation. **FeTHT** displays prominent peaks at 1.21°, 2.18°, 2.42°, and 3.21°, and a broad peak at 7.09° (Figure 1). These peaks are similar to the ones reported for the **CoTHT** framework, suggesting analogous structural environments for the Co and Fe systems.[52,69] The peak at 1.21° corresponds to the [100] reflection and is indicative of a pore diameter of approximately 2.0 nm. This pore diameter is consistent with the recently reported PXRD pattern of $Fe_3(THT)_2(NH_4)_3$ (~1.9 nm), confirming that the modified synthetic procedure employed here enables exclusion of the ammonium guest species without substantially altering the 2D structure of the material.[55] Figure 1 illustrates a comparison of the experimentally observed diffraction pattern of **FeTHT** with the simulated pattern of a model using the *P6/mmm* space group and unit cell parameters of $a = b = 22.52$ Å and $c = 3.34$ Å (Figure S1). This diffraction data indicates good long-range order in the *ab* plane and weak ordering along the *c* axis. The morphology of **FeTHT** films was examined using scanning electron microscopy (SEM). Low magnification images (Figure 1, inset) show few cracks, and higher magnification images (Figure S2) reveal flat, sheet-like morphologies consistent with images of similar 2D MOFs. Nitrogen gas sorption isotherms show that **FeTHT** has a Brunauer−Emmett−Teller (BET) surface area of 441 m^2/g (Figure S3), which is similar to the surface areas reported for analogous cobalt and iron THT frameworks of 370 and 526 m^2/g, respectively.[52,55]

Following exposure of the frameworks to air (3 days at 60 °C), the PXRD pattern of **FeTHT** samples show the strong peaks at 1.21°, 2.18°, 2.42°, 3.21° in the as-prepared sample (Figures S4−S6) are maintained after exposure to the atmosphere. The broad peak at 7.09° shifts to lower angles and sharpens to reveal features consistent with the simulated spectrum, suggesting more structural order in the *c*-direction. Upon cooling, a decrease in interlayer distance is observed for the [001] reflection (from 3.34 to3.23 Å), however the [100] reflection remains unchanged (Figure S5). No significant change in film thickness or morphology was observed by AFM after oxidation of the framework (Figure S7). The measured BET surface area of the oxidized **FeTHT** sample was determined to be 27.6 m^2/g (Figure S8), indicating a significant loss of accessible surface area. A similar reduction in the available surface area from 370 to 50 m^2/g was previously reported for $Fe(tri)_2$ MOF upon oxidation, where tri = 1,2,3-triazolate, and was attributed to occupation of the pores by charge-balancing species (BF_4^-).[26]

Density Functional Theory (DFT) Calculations. To understand the electronic structure of the **FeTHT** framework in the absence of ammonium guest species, first-principles calculations were carried out on the modeled structure using plane-wave DFT (see the Supporting Information for details). The calculations predict a ground-state magnetization density with one unpaired electron per Fe ion, consistent with Fe^{3+} in a distorted-octahedral crystal field. A strong preference for ferromagnetic coupling between layers and a weaker frustrated antiferromagnetic coupling within the 2D sheets produces a net magnetic moment of 2.2 μ_B per unit cell. The predicted equilibrium geometry is in good agreement with the experimentally measured lattice parameters, and similar results were obtained from DFT+*U* calculations with a Hubbard *U* correction of 5 eV applied to the Fe d orbitals.

As in our previous calculations on the analogous **CoTHT** framework,[52] the band dispersion suggests that bulk **FeTHT** is a semimetal with a small density of states at the Fermi energy (Figure 2). These states are primarily composed of Fe d and S p, with a strong interlayer interaction along the *c*-axis,

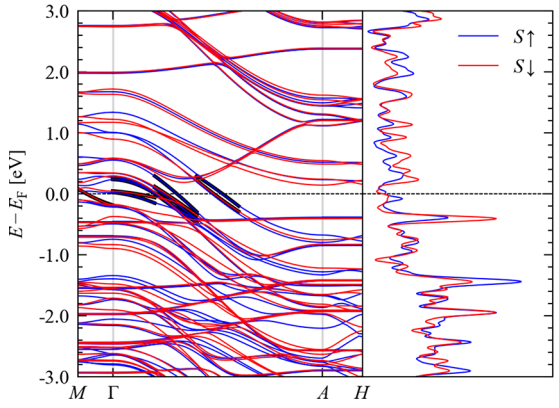

Figure 2. Calculated band dispersion and electronic density of states curves for the **FeTHT** framework with no guest species. The blue and red lines denote electronic states in the "up" and "down" spin channels. The thick black lines mark the regions of the dispersion used to evaluate $\partial^2 E(k)/\partial k^2$ to estimate the carrier effective masses discussed in the text.

DOI: 10.1021/jacs.9b06898
J. Am. Chem. Soc. 2019, 141, 16323−16330

corresponding to the Γ-*A* segment of the band structure, which shows a significant dispersion of ∼1.8 eV. Carrier effective masses ranging from 0.55 to 6.72 m_e were estimated from the band dispersion, which are comparable to the values of 0.29−8.04 m_e predicted for the **CoTHT** analogue.[52] The band dispersion also shows a small number of metallic states along the *M*−Γ segment, corresponding to in-plane conductivity, with a carrier mass around 0.99 m_e. Semimetallic electronic structures were also predicted for both the **FeTHT** and **CoTHT** frameworks with DFT+*U* calculations, which provide confidence that these results are not an artifact of unphysical delocalization of the Fe d electrons. Prior electronic-structure calculations on the **FeTHT** framework with explicit ammonium guest molecules predict a narrow bandgap (∼350 meV),[55] highlighting the sensitivity of the electronic structure to subtle environmental factors. The predicted elimination of this gap upon removal of the NH_4^+ provides a strong indication that the modified **FeTHT** reported here should exhibit distinct electronic behavior relative to the previously reported semiconducting **FeTHT**.

Computational studies of the $Ni_3(HITP)_2$ framework[44] reported that a staggered arrangement of the layers has the lowest total energy compared to an eclipsed geometry, whereas our previous calculations on the **CoTHT** framework found the latter to be lowest in energy.[52] The calculated potential-energy surface for stacking faults in **FeTHT** (Figure 3) shows that

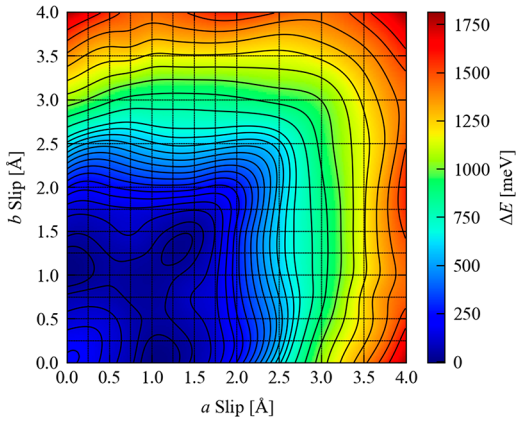

Figure 3. Calculated DFT potential-energy surface associated with layer offsets (stacking faults) in the pristine **FeTHT** framework.

layer offsets of ∼1.0−1.25 Å along the *a*/*b* axis or a combined offset of 1.25 Å along both axes are lower in energy than the eclipsed configuration by Δ*E* = 83 and 98 meV per Fe ion, respectively. These small energy differences between the two configurations suggest that formation of stacking faults in **FeTHT** is likely to be somewhat facile, which is consistent with the broad [001] PXRD peak observed. Earlier calculations on the **FeTHT** framework with ammonium guest species suggest that an inclined AA-stacked geometry is the most stable, which is consistent with our results.[55] As for the **CoTHT** framework, the calculations predict that the stacking faults would reduce the density of states around the Fermi energy and introduce a gap into the conduction band, both of which are intuitive given the nature of the metallic states. Intrinsic stacking faults, as well as environmental factors, may play key roles in defining the electronic structure of **FeTHT** and inducing a semiconductor-to-metal transition.

X-ray Photoelectron Spectroscopy (XPS) and Magnetism Studies. The surface composition of the **FeTHT** films was investigated using X-ray photoelectron spectroscopy (XPS). Survey scans of pristine **FeTHT** films reveal the presence of Fe, S, C, and O. Fitting of the Fe 2p, shown in Figure 4a, was primarily based on the Fe 2p multiplet splitting of Fe_3O_4 which was used as a reference.[70] The peaks at binding energies of 708.2, 709.2, and 710.3 eV are assigned to Fe^{2+}, and the peaks at 710.1, 711.2, 712.3, and 713.5 eV are assigned to Fe^{3+} (see Table S5). The Fe 2p region shows mixed $Fe^{3+/2+}$ valency with approximately 52% Fe^{2+} and 48% Fe^{3+}; indicating the presence of mixed oxidation states in pristine **FeTHT**.[23] Figure 4b shows peak fitting of the S 2p regions for the pristine sample. The binding energy difference of the S $2p_{3/2}$−S $2p_{1/2}$ doublet was fixed to 1.2 eV with intensity ratio 2:1.[71,72]

Examination of the same XPS regions in a sample after prolonged air exposure reveals distinct changes in the Fe 2p and S 2p regions. Following 7 days of exposure to ambient atmosphere, the first peak of the Fe^{2+} multiplet disappears and the experimental data can be fit by the Fe^{3+} multiplet alone (Figure 4a), indicating complete surface oxidation of the metal sites. In the S 2p region, two new sets of peaks appear at higher binding energies of ∼166 and ∼168 eV, indicating concomitant ligand oxidation (Figure 4b). These environments are attributed to sulfenate and sulfinate moieties, as previously reported in a palladium dithiolene molecular complex.[73] To further substantiate these assignments, high resolution XPS of the corresponding Pd and Fe molecular species have been collected before and after O_2 exposure (Figure S18−S21). The S 2p region of the previously reported palladium coordination polymers confirms that aerobic oxidation results in a new oxidized sulfur-containing moiety, which appears at ∼167 eV (Figures S20 and S21).[73] This new feature was assigned as the added presence of sulfenate/sulfinate moieties, which was confirmed by the reported crystal structure of the resulting Pd polymer.[73] Likewise, aerobic oxidation of the analogous iron dithiolene complex reproduces the additional S 2p features observed for the **FeTHT** framework, which supports the assignment of these new features as sulfenate/sulfinate moieties (Figures S18 and S19). By examining the area of the peaks in the O_2-exposed **FeTHT** sample (Figure 4b), approximately 49% of the thiolate moieties appear to be oxidized, with a sulfenate:sulfinate ratio of 1:4. These numbers are similar to the reported Pd dithiolene complex, in which half of all thiolates are oxidized, with a sulfenate/sulfinate ratio of 1:2.3.[73]

These XPS results thus confirm that both the metal center and the ligand backbone are oxidized after prolonged exposure to air. This is consistent with the predominant contributions from interacting Fe and S orbitals to the partially occupied bands predicted by DFT. The calculations also reveal a preference for an offset rather than eclipsed layer stacking, indicating that interlayer Fe−S interactions may play a role in directing stacking manifolds. As these are expected to be weak interactions, based on the predicted ease of generating stacking faults, the formation of new S−O bonds upon oxidation may facilitate stronger Fe−O interlayer interactions, consistent with the sharpening of the peak at 7.09° by synchrotron PXRD. As no such oxidized thiolate moieties were evident in the **CoTHT** material, we attribute the thickness-dependence of the cobalt system to a slower oxidation process relative to the analogous iron-containing framework.[51]

DOI: 10.1021/jacs.9b06898
J. Am. Chem. Soc. 2019, 141, 16323−16330

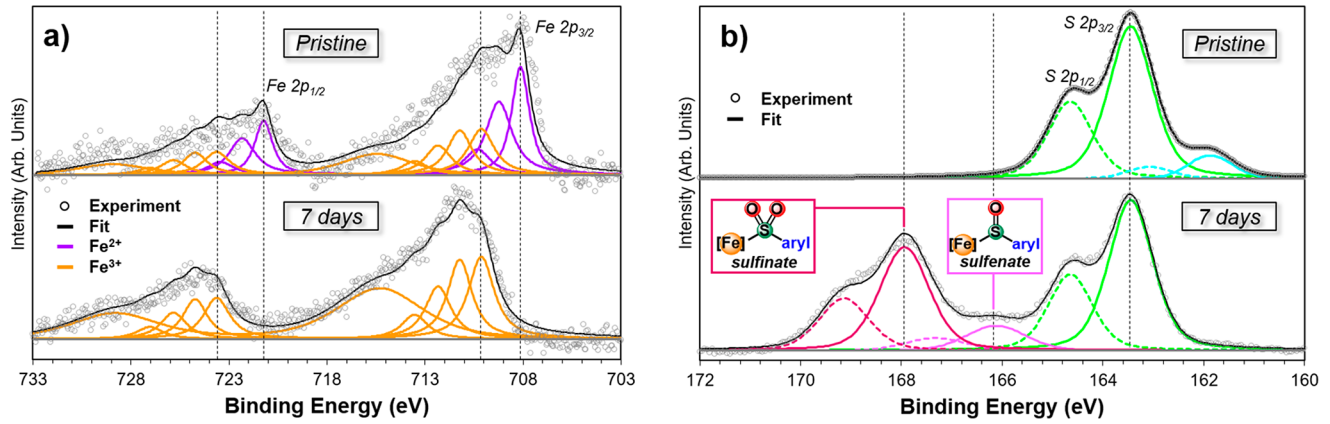

Figure 4. Fitting of the XPS spectra of pristine **FeTHT** and samples exposed to ambient atmosphere for 7 days. (a) Fe 2p region showing mixed valency ($Fe^{2+/3+}$) in pristine **FeTHT**; after exposure to air, only the Fe^{3+} peak is observed. (b) S 2p region in the pristine **FeTHT**; after exposure to air, two new doublets at ~166 (pink) and ~168 eV (burgundy) appear, in addition to the original features for the pristine FeTHT (green), indicating the formation of dithiolene moieties with different degrees of oxidation.

To evaluate the mixture of iron oxidation states in bulk **FeTHT**, magnetic measurements were performed. It was previously reported that mixed-valency in MOFs can enhance conductivity by promoting charge hopping.[74] Recent studies of iron-based 3D MOFs have shown that controlling mixed-valency at Fe sites can have dramatic effects on the bulk transport properties, increasing conductivity by as many as 8 orders of magnitude.[25,26,75] By examining the saturation of unpaired spins in the hysteresis loop in **FeTHT** (Figure S22b), it is estimated that 33% of the iron centers are Fe^{3+}, with the remaining 67% Fe^{2+}. These results are in agreement with the XPS studies, as similar mixed $Fe^{3+/2+}$ valency is observed in the as-prepared **FeTHT** material, albeit a higher degree of oxidation is estimated by XPS (1:1 from XPS studies vs 2:1 from magnetic studies). The higher degree of oxidation observed by XPS suggests that the oxidized species are concentrated toward the surface of the sample, as magnetic and XPS measurements analyze the bulk vs surface composition, respectively. After exposure of the **FeTHT** to air for 3 days at 60 °C, the observed magnetic moment of the sample increases, which is consistent with oxidation to give an increased amount of Fe^{3+} (Figure S22a). This increased moment reflects an increase of the Fe^{2+}/Fe^{3+} ratio from 2:1 to 1:1. The magnetic studies thus indicate a slightly lower degree of oxidation of **FeTHT** compared to the results from the XPS studies (only Fe^{3+} is detected by XPS upon exposure of the sample to ambient atmosphere for 7 days). These results demonstrate O_2-treatment as an accessible tool for surface-localized chemical oxidation of 2D MOFs.

Resistivity Studies. The temperature-dependent resistivity of **FeTHT** was measured using a four-point Van der Pauw geometry. Films of thicknesses ranging from 84(8) nm to 410(41) nm, as determined by AFM studies (Figure S24), were analyzed under identical conditions. Ohmic contacts, as demonstrated by linear I–V traces (Figure S25), were made using graphitic carbon adhesive in ambient atmosphere with minimal (<10 min) air exposure. At 300 K, the bulk resistivity of the 275 nm-thick **FeTHT** film was determined to be 5.4 Ω·cm, corresponding to a conductivity of 0.2 S/cm (Figures 5 and S26 and Table S7). Cooling from 300 to 140 K results in an increased resistivity, as expected for a semiconducting material where transport is dominated by thermally populated carriers (Figures 5 and S26). This is similar to what was

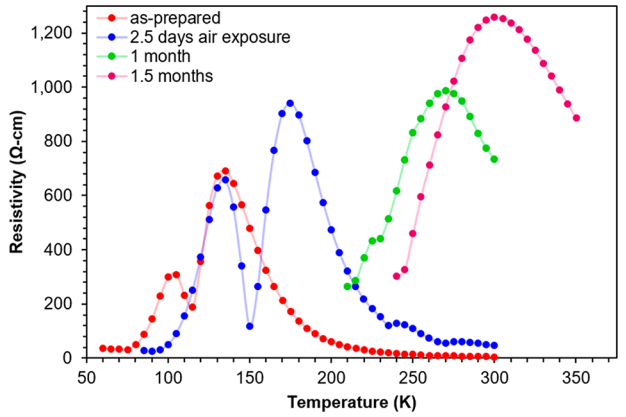

Figure 5. Temperature-dependent resistivity data for **FeTHT** films with 275(28) nm thickness, as-prepared with minimal (<10 min) air exposure (red) and following exposure to ambient atmosphere for 2.5 days (blue), 1 month (green), and 1.5 months (magenta).

observed for films and pressed pellets of **CoTHT** at elevated temperatures and is consistent with the report of semiconducting behavior for $Fe_3(THT)_2(NH_4)_3$ (Table S8).[52,55] An Arrhenius fit to the resistivity data recorded between 300 and 200 K indicates an activation energy for electron hopping between 6 and 13 meV (Figures S27 and S28), which suggests defects, most likely grain boundaries in the 2D sheets, significantly influence the charge transport.

Below 140 K, the **FeTHT** film exhibits a maximum in the resistivity followed by a change in slope to decrease below 100 K (Figures 5 and S26 and Table S7). These observations are qualitatively very similar to the behavior of **CoTHT**,[52] and are fully reversible with no signatures of thermal hysteresis. Given the complex nature of the transition, $T_{metallic}$ is defined as the lowest transition temperature at which **FeTHT** becomes metallic (100 K). No morphological changes are observed by scanning electron microscopy (Figure S29). The measured semiconductor-to-metal transition temperatures ($T_{metallic}$) for **FeTHT** do not display any appreciable shifts with film thickness (Figure S26 and Table S7).

To further examine the influence that oxidation has on the conductivity, resistivity measurements were collected on samples exposed to air for various durations. The original 275(28) nm-thick **FeTHT** film was exposed to the ambient

DOI: 10.1021/jacs.9b06898
J. Am. Chem. Soc. 2019, 141, 16323–16330

atmosphere, while taking care to maintain the original contacts. After two and a half days of exposure, the resistivity was observed to increase nearly 10-fold, from 5.2 to 47.5 Ω·cm at 300 K (Figure 5). Remarkably, this coincides with a signficant increase in the maxima of the resisitivity from 100 to 135 K. Further oxidation over a one month period led to a shift to approximately 300 K with a corresponding increase in resistivity to 735 Ω·cm. By one and a half months, the transition was shifted to room temperature and exhibited a $\rho_{300\ K}$ of 1260 Ω·cm. These effects were seen to accelerate when a 310(31) nm-thick sample of **FeTHT** was heated in air at 60 °C for 3 days (Figure S30). In contrast, heating the sample for the same duration under helium shows nearly no change in the position of the maxima (Figure S31), which supports the conclusion that the shifts in the transition temperature are related to the oxidation of Fe^{2+} to Fe^{3+}.

CONCLUSIONS

We have presented a modified synthesis for the recently reported iron 2,3,6,7,10,11-tripheylenehexathiolate (**FeTHT**) MOF, generating a material with unusual electronic properties that is isostructural to the previously reported **CoTHT**. Temperature-dependent resistivity studies reveal a transition from semiconducting to metallic character on cooling, which is analogous to the behavior observed for **CoTHT**. This contrasts with previously reported measurements on **FeTHT** where NH_4^+ was present as a guest species and exhibited purely semiconducting behavior. Interestingly, oxidation of the material on exposure to ambient conditions has a significant effect on the semiconducting-to-metallic transition temperature over time, resulting in a material with metallic-like behavior at room temperature. Through a combination of X-ray photoelectron spectroscopy (XPS) and magnetic susceptibility studies, we have shown that both the metal center and the ligand backbone are susceptible to oxidation. These results indicate the semiconducting-to-metallic transition is strongly influenced by changes in the degree of doping of the material and provides greater insight into the possible origin of this behavior.

ASSOCIATED CONTENT

Supporting Information

The Supporting Information is available free of charge on the ACS Publications website at DOI: 10.1021/jacs.9b06898.

Experimental methods, synthetic procedures, computational methods and results, elemental analysis, SEM images, BET results, PXRD data, XPS data, magnetism and conductivity data, and corresponding tabulated results (PDF)

AUTHOR INFORMATION

Corresponding Authors

*melot@usc.edu

*smarines@usc.edu

ORCID

Nicholas M. Orchanian: 0000-0001-5752-6845

Jonathan M. Skelton: 0000-0002-0395-1202

Courtney A. Downes: 0000-0001-8631-1579

Louis F. J. Piper: 0000-0002-3421-3210

Aron Walsh: 0000-0001-5460-7033

Brent C. Melot: 0000-0002-7078-8206

Smaranda C. Marinescu: 0000-0003-2106-8971

Notes

The authors declare no competing financial interest.

ACKNOWLEDGMENTS

We are grateful to the University of Southern California (USC) and the USC Women in Science and Engineering for funding. A.J.C. gratefully acknowledges support from the Norma and Jerol Sonosky Fellowship and the USC Wrigley Institute. A.J.N and B.C.M. gratefully acknowledge funding through Office of Naval Research Grant No. N00014-15-1-2411. S.A.H. was supported as part of the Multidisciplinary GAANN in Smart Energy Materials, a Graduate Areas of National Need, funded by the U.S. Department of Education, under Award P200A150135. J.M.S. is grateful to the UK Engineering and Physical Sciences Council (Grant No. EP/P007821/1) and to the University of Manchester for the support of a Presidential Fellowship. SEM data were collected at the Center for Electron Microscopy and Microanalysis (CEMMA), USC. Use of the Advanced Photon Source at Argonne National Laboratory was supported by the U.S. Department of Energy, Office of Science, Office of Basic Energy Sciences, under Contract No. DE-AC02-06CH11357. We are grateful to Prof. Mark Thompson for allowing the use of the Agilent 5420 SPM instrument for AFM studies. We thank Sara Smock for assistance with the BET measurements. The computational modelling studies were carried out using the UK Archer HPC facility through the UK Materials Chemistry Consortium, which is funded by the EPSRC (Grant. No. EP/L000202).

REFERENCES

(1) Furukawa, H.; Cordova, K. E.; O'Keeffe, M.; Yaghi, O. M. The Chemistry and Applications of Metal-Organic Frameworks. *Science* **2013**, *341*, 1230444.

(2) Zhou, H.-C.; Long, J. R.; Yaghi, O. M. Introduction to Metal–Organic Frameworks. *Chem. Rev.* **2012**, *112*, 673–674.

(3) Allendorf, M. D.; Stavila, V. Crystal engineering, structure-function relationships, and the future of metal-organic frameworks. *CrystEngComm* **2015**, *17*, 229–246.

(4) Meek, S. T.; Greathouse, J. A.; Allendorf, M. D. Metal-Organic Frameworks: A Rapidly Growing Class of Versatile Nanoporous Materials. *Adv. Mater.* **2011**, *23*, 249–267.

(5) Hendon, C. H.; Rieth, A. J.; Korzyński, M. D.; Dincă, M. Grand Challenges and Future Opportunities for Metal–Organic Frameworks. *ACS Cent. Sci.* **2017**, *3*, 554–563.

(6) Liu, G.; Chernikova, V.; Liu, Y.; Zhang, K.; Belmabkhout, Y.; Shekhah, O.; Zhang, C.; Yi, S.; Eddaoudi, M.; Koros, W. J. Mixed matrix formulations with MOF molecular sieving for key energy-intensive separations. *Nat. Mater.* **2018**, *17*, 283–289.

(7) Qiu, S.; Xue, M.; Zhu, G. Metal-organic framework membranes: from synthesis to separation application. *Chem. Soc. Rev.* **2014**, *43*, 6116–6140.

(8) Schoedel, A.; Ji, Z.; Yaghi, O. M. The role of metal–organic frameworks in a carbon-neutral energy cycle. *Nat. Energy* **2016**, *1*, 16034.

(9) Zhang, T.; Lin, W. Metal-organic frameworks for artificial photosynthesis and photocatalysis. *Chem. Soc. Rev.* **2014**, *43*, 5982–5993.

(10) Yaghi, O. M.; O'Keeffe, M.; Ockwig, N. W.; Chae, H. K.; Eddaoudi, M.; Kim, J. Reticular synthesis and the design of new materials. *Nature* **2003**, *423*, 705–714.

(11) Sun, L.; Campbell, M. G.; Dincă, M. Electrically Conductive Porous Metal–Organic Frameworks. *Angew. Chem., Int. Ed.* **2016**, *55*, 3566–3579.

DOI: 10.1021/jacs.9b06898
J. Am. Chem. Soc. 2019, 141, 16323–16330

(12) Stassen, I.; Burtch, N.; Talin, A.; Falcaro, P.; Allendorf, M.; Ameloot, R. An updated roadmap for the integration of metal-organic frameworks with electronic devices and chemical sensors. *Chem. Soc. Rev.* **2017**, *46*, 3185−3241.
(13) Downes, C. A.; Marinescu, S. C. Electrocatalytic Metal−Organic Frameworks for Energy Applications. *ChemSusChem* **2017**, *10*, 4374−4392.
(14) Hendon, C. H.; Tiana, D.; Walsh, A. Conductive metal-organic frameworks and networks: fact or fantasy? *Phys. Chem. Chem. Phys.* **2012**, *14*, 13120−13132.
(15) Allendorf, M. D.; Schwartzberg, A.; Stavila, V.; Talin, A. A. A Roadmap to Implementing Metal−Organic Frameworks in Electronic Devices: Challenges and Critical Directions. *Chem. - Eur. J.* **2011**, *17*, 11372−11388.
(16) Kung, C.-W.; Otake, K.; Buru, C. T.; Goswami, S.; Cui, Y.; Hupp, J. T.; Spokoyny, A. M.; Farha, O. K. Increased Electrical Conductivity in a Mesoporous Metal−Organic Framework Featuring Metallacarboranes Guests. *J. Am. Chem. Soc.* **2018**, *140*, 3871−3875.
(17) Talin, A. A.; Centrone, A.; Ford, A. C.; Foster, M. E.; Stavila, V.; Haney, P.; Kinney, R. A.; Szalai, V.; El Gabaly, F.; Yoon, H. P.; Léonard, F.; Allendorf, M. D. Tunable Electrical Conductivity in Metal-Organic Framework Thin-Film Devices. *Science* **2014**, *343*, 66−69.
(18) Mulzer, C. R.; Shen, L.; Bisbey, R. P.; McKone, J. R.; Zhang, N.; Abruña, H. D.; Dichtel, W. R. Superior Charge Storage and Power Density of a Conducting Polymer-Modified Covalent Organic Framework. *ACS Cent. Sci.* **2016**, *2*, 667−673.
(19) Kobayashi, Y.; Jacobs, B.; Allendorf, M. D.; Long, J. R. Conductivity, Doping, and Redox Chemistry of a Microporous Dithiolene-Based Metal−Organic Framework. *Chem. Mater.* **2010**, *22*, 4120−4122.
(20) Cai, S.-L.; Zhang, Y.-B.; Pun, A. B.; He, B.; Yang, J.; Toma, F. M.; Sharp, I. D.; Yaghi, O. M.; Fan, J.; Zheng, S.-R.; Zhang, W.-G.; Liu, Y. Tunable electrical conductivity in oriented thin films of tetrathiafulvalene-based covalent organic framework. *Chem. Sci.* **2014**, *5*, 4693−4700.
(21) Cui, J.; Xu, Z. An electroactive porous network from covalent metal−dithiolene links. *Chem. Commun.* **2014**, *50*, 3986−3988.
(22) Murase, R.; Leong, C. F.; D'Alessandro, D. M. Mixed Valency as a Strategy for Achieving Charge Delocalization in Semiconducting and Conducting Framework Materials. *Inorg. Chem.* **2017**, *56*, 14373−14382.
(23) Sun, L.; Hendon, C. H.; Park, S. S.; Tulchinsky, Y.; Wan, R.; Wang, F.; Walsh, A.; Dincă, M. Is iron unique in promoting electrical conductivity in MOFs? *Chem. Sci.* **2017**, *8*, 4450−4457.
(24) Manumpil, M. A.; Leal-Cervantes, C.; Hudson, M. R.; Brown, C. M.; Karunadasa, H. I. Electronic Conductivity in a Porous Vanadyl Prussian Blue Analogue upon Air Exposure. *Inorg. Chem.* **2017**, *56*, 12682−12686.
(25) Xie, L. S.; Sun, L.; Wan, R.; Park, S. S.; DeGayner, J. A.; Hendon, C. H.; Dincă, M. Tunable Mixed-Valence Doping toward Record Electrical Conductivity in a Three-Dimensional Metal−Organic Framework. *J. Am. Chem. Soc.* **2018**, *140*, 7411−7414.
(26) Park, J. G.; Aubrey, M. L.; Oktawiec, J.; Chakarawet, K.; Darago, L. E.; Grandjean, F.; Long, G. J.; Long, J. R. Charge Delocalization and Bulk Electronic Conductivity in the Mixed-Valence Metal−Organic Framework $Fe(1,2,3\text{-triazolate})_2(BF_4)_x$. *J. Am. Chem. Soc.* **2018**, *140*, 8526−8534.
(27) Narayan, T. C.; Miyakai, T.; Seki, S.; Dincă, M. High Charge Mobility in a Tetrathiafulvalene-Based Microporous Metal−Organic Framework. *J. Am. Chem. Soc.* **2012**, *134*, 12932−12935.
(28) Park, S. S.; Hontz, E. R.; Sun, L.; Hendon, C. H.; Walsh, A.; Van Voorhis, T.; Dincă, M. Cation-Dependent Intrinsic Electrical Conductivity in Isostructural Tetrathiafulvalene-Based Microporous Metal−Organic Frameworks. *J. Am. Chem. Soc.* **2015**, *137*, 1774−1777.
(29) Sun, L.; Miyakai, T.; Seki, S.; Dincă, M. Mn_2(2,5-disulfhydrylbenzene-1,4-dicarboxylate): A Microporous Metal−Organic Framework with Infinite (−Mn−S−)∞ Chains and High Intrinsic Charge Mobility. *J. Am. Chem. Soc.* **2013**, *135*, 8185−8188.
(30) Ko, M.; Mendecki, L.; Mirica, K. A. Conductive two-dimensional metal−organic frameworks as multifunctional materials. *Chem. Commun.* **2018**, *54*, 7873−7891.
(31) D'Alessandro, D. M. Exploiting redox activity in metal−organic frameworks: concepts, trends and perspectives. *Chem. Commun.* **2016**, *52*, 8957−8971.
(32) Maeda, H.; Sakamoto, R.; Nishihara, H. Coordination Programming of Two-Dimensional Metal Complex Frameworks. *Langmuir* **2016**, *32*, 2527−2538.
(33) Sakamoto, R.; Takada, K.; Pal, T.; Maeda, H.; T, K.; Nishihara, H. Coordination nanosheets (CONASHs): strategies, structures and functions. *Chem. Commun.* **2017**, *53*, 5781−5801.
(34) Calbo, J.; Golomb, M. J.; Walsh, A. Redox-active metal-organic frameworks for energy conversion and storage. *J. Mater. Chem. A* **2019**, *7*, 16571−16597.
(35) Darago, L. E.; Aubrey, M. L.; Yu, C. J.; Gonzalez, M. I.; Long, J. R. Electronic Conductivity, Ferrimagnetic Ordering, and Reductive Insertion Mediated by Organic Mixed-Valence in a Ferric Semiquinoid Metal−Organic Framework. *J. Am. Chem. Soc.* **2015**, *137*, 15703−15711.
(36) Ziebel, M. E.; Darago, L. E.; Long, J. R. Control of Electronic Structure and Conductivity in Two-Dimensional Metal−Semiquinoid Frameworks of Titanium, Vanadium, and Chromium. *J. Am. Chem. Soc.* **2018**, *140*, 3040−3051.
(37) Hmadeh, M.; Lu, Z.; Liu, Z.; Gándara, F.; Furukawa, H.; Wan, S.; Augustyn, V.; Chang, R.; Liao, L.; Zhou, F.; Perre, E.; Ozolins, V.; Suenaga, K.; Duan, X.; Dunn, B.; Yamamto, Y.; Terasaki, O.; Yaghi, O. M. New Porous Crystals of Extended Metal-Catecholates. *Chem. Mater.* **2012**, *24*, 3511−3513.
(38) Park, J.; Hinckley, A. C.; Huang, Z.; Feng, D.; Yakovenko, A. A.; Lee, M.; Chen, S.; Zou, X.; Bao, Z. Synthetic Routes for a 2D Semiconductive Copper Hexahydroxybenzene Metal−Organic Framework. *J. Am. Chem. Soc.* **2018**, *140*, 14533−14537.
(39) Hoppe, B.; Hindricks, K. D. J.; Warwas, D. P.; Schulze, H. A.; Mohmeyer, A.; Pinkvos, T. J.; Zailskas, S.; Krey, M. R.; Belke, C.; König, S.; Fröba, M.; Haug, R. J.; Behrens, P. Graphene-like metal−organic frameworks: morphology control, optimization of thin film electrical conductivity and fast sensing applications. *CrystEngComm* **2018**, *20*, 6458−6471.
(40) Campbell, M. G.; Liu, S. F.; Swager, T. M.; Dincă, M. Chemiresistive Sensor Arrays from Conductive 2D Metal−Organic Frameworks. *J. Am. Chem. Soc.* **2015**, *137*, 13780−13783.
(41) Yao, M.-S.; Lv, X.-J.; Fu, Z.-H.; Li, W.-H.; Deng, W.-H.; Wu, G.-D.; Xu, G. Layer-by-Layer Assembled Conductive Metal−Organic Framework Nanofilms for Room-Temperature Chemiresistive Sensing. *Angew. Chem., Int. Ed.* **2017**, *56*, 16510−16514.
(42) Rubio-Gimenez, V. c.; Galbiati, M.; Castells-Gil, J.; Almora-Barrios, N.; Navarro-Sanchez, J.; Escorcia-Ariza, G.; Mattera, M.; Arnold, T.; Rawle, J.; Tatay, S.; Coronado, E.; Marti-Gastaldo, C. Bottom-Up Fabrication of Semiconductive Metal−Organic Framework Ultrathin Films. *Adv. Mater.* **2018**, *30*, 1704291.
(43) Ko, M.; Aykanat, A.; Smith, M. K.; Mirica, K. A. Drawing Sensors with Ball-Milled Blends of Metal-Organic Frameworks and Graphite. *Sensors* **2017**, *17*, 2192.
(44) Sheberla, D.; Sun, L.; Blood-Forsythe, M. A.; Er, S.; Wade, C. R.; Brozek, C. K.; Aspuru-Guzik, A.; Dincă, M. High Electrical Conductivity in Ni_3(2,3,6,7,10,11-hexaiminotriphenylene)$_2$, a Semiconducting Metal−Organic Graphene Analogue. *J. Am. Chem. Soc.* **2014**, *136*, 8859−8862.
(45) Sun, L.; Liao, B.; Sheberla, D.; Kraemer, D.; Zhou, J.; Stach, E. A.; Zakharov, D.; Stavila, V.; Talin, A. A.; Ge, Y.; Allendorf, M. D.; Chen, G.; Léonard, F.; Dincă, M. A Microporous and Naturally Nanostructured Thermoelectric Metal-Organic Framework with Ultralow Thermal Conductivity. *Joule* **2017**, *1*, 168−177.
(46) Dou, J.-H.; Sun, L.; Ge, Y.; Li, W.; Hendon, C. H.; Li, J.; Gul, S.; Yano, J.; Stach, E. A.; Dincă, M. Signature of Metallic Behavior in

DOI: 10.1021/jacs.9b06898
J. Am. Chem. Soc. 2019, 141, 16323−16330

the Metal−Organic Frameworks M_3(hexaiminobenzene)$_2$ (M = Ni, Cu). *J. Am. Chem. Soc.* **2017**, *139*, 13608−13611.
(47) Feng, D.; Lei, T.; Lukatskaya, M. R.; Park, J.; Huang, Z.; Lee, M.; Shaw, L.; Chen, S.; Yakovenko, A. A.; Kulkarni, A.; Xiao, J.; Fredrickson, K.; Tok, J. B.; Zou, X.; Cui, Y.; Bao, Z. Robust and conductive two-dimensional metal− organic frameworks with exceptionally high volumetric and areal capacitance. *Nat. Energy* **2018**, *3*, 30−36.
(48) Park, J.; Lee, M.; Feng, D.; Huang, Z.; Hinckley, A. C.; Yakovenko, A.; Zou, X.; Cui, Y.; Bao, Z. Stabilization of Hexaaminobenzene in a 2D Conductive Metal− Organic Framework for High Power Sodium Storage. *J. Am. Chem. Soc.* **2018**, *140*, 10315−10323.
(49) Huang, X.; Sheng, P.; Tu, Z.; Zhang, F.; Wang, J.; Geng, H.; Zou, Y.; Di, C.-a.; Yi, Y.; Sun, Y.; Xu, W.; Zhu, D. A two-dimensional π−d conjugated coordination polymer with extremely high electrical conductivity and ambipolar transport behaviour. *Nat. Commun.* **2015**, *6*, 7408.
(50) Kambe, T.; Sakamoto, R.; Kusamoto, T.; Pal, T.; Fukui, N.; Hoshiko, K.; Shimojima, T.; Wang, Z.; Hirahara, T.; Ishizaka, K.; Hasegawa, S.; Liu, F.; Nishihara, H. Redox Control and High Conductivity of Nickel Bis(dithiolene) Complex π-Nanosheet: A Potential Organic Two-Dimensional Topological Insulator. *J. Am. Chem. Soc.* **2014**, *136*, 14357−14360.
(51) Sun, X.; Wu, K.-H.; Sakamoto, R.; Kusamoto, T.; Maeda, H.; Ni, X.; Jiang, W.; Liu, F.; Sasaki, S.; Masunaga, H.; Nishihara, H. Bis(aminothiolato)nickel nanosheet as a redox switch for conductivity and an electrocatalyst for the hydrogen evolution reaction. *Chem. Sci.* **2017**, *8*, 8078−8085.
(52) Clough, A. J.; Skelton, J. M.; Downes, C. A.; de la Rosa, A. A.; Yoo, J. W.; Walsh, A.; Melot, B. C.; Marinescu, S. C. Metallic Conductivity in a Two-Dimensional Cobalt Dithiolene Metal−Organic Framework. *J. Am. Chem. Soc.* **2017**, *139*, 10863−10867.
(53) Takaishi, S.; Hosoda, M.; Kajiwara, T.; Miyasaka, H.; Yamashita, M.; Nakanishi, Y.; Kitagawa, Y.; Yamaguchi, K.; Kobayashi, A.; Kitagawa, H. Electroconductive Porous Coordination Polymer Cu[Cu(pdt)$_2$] Composed of Donor and Acceptor Building Units. *Inorg. Chem.* **2009**, *48*, 9048−9050.
(54) Kambe, T.; Sakamoto, R.; Hoshiko, K.; Takada, K.; Miyachi, M.; Ryu, J.-H.; Sasaki, S.; Kim, J.; Nakazato, K.; Takata, M.; Nishihara, H. π-Conjugated Nickel Bis(dithiolene) Complex Nanosheet. *J. Am. Chem. Soc.* **2013**, *135*, 2462−2465.
(55) Dong, R.; Han, P.; Arora, H.; Ballabio, M.; Karakus, M.; Zhang, Z.; Shekhar, C.; Adler, P.; Petkov, P. S.; Erbe, A.; Mannsfeld, S. C. B.; Felser, C.; Heine, T.; Bonn, M.; Feng, X.; Canovas, E. High-mobility band-like charge transport in a semiconducting two-dimensional metal−organic framework. *Nat. Mater.* **2018**, *17*, 1027−1032.
(56) Sun, X.; Wu, K.-H.; Sakamoto, R.; Kusamoto, T.; Maeda, H.; Nishihara, H. Conducting π-Conjugated Bis(iminothiolato)nickel Nanosheet. *Chem. Lett.* **2017**, *46*, 1072−1075.
(57) Dong, R.; Zhang, Z.; Tranca, D. C.; Zhou, S.; Wang, M.; Adler, P.; Liao, Z.; Liu, F.; Sun, Y.; Shi, W.; Zhang, Z.; Zschech, E.; Mannsfeld, S. C. B.; Felser, C.; Feng, X. A coronene-based semiconducting two- dimensional metal-organic framework with ferromagnetic behavior. *Nat. Commun.* **2018**, *9*, 2637.
(58) Huang, X.; Li, H.; Tu, Z.; Liu, L.; Wu, X.; Chen, J.; Liang, Y.; Zou, Y.; Yi, Y.; Sun, J.; Xu, W.; Zhu, D. Highly Conducting Neutral Coordination Polymer with Infinite Two- Dimensional Silver−Sulfur Networks. *J. Am. Chem. Soc.* **2018**, *140*, 15153−15156.
(59) Chen, I.-F.; Lu, C.-F.; Su, W.-F. Highly Conductive 2D Metal−Organic Framework Thin Film Fabricated by Liquid−Liquid Interfacial Reaction Using One-Pot- Synthesized Benzenehexathiol. *Langmuir* **2018**, *34*, 15754−15762.
(60) Pal, T.; Doi, S.; Maeda, H.; Wada, K.; Tan, C. M.; Fukui, N.; Sakamoto, R.; Tsuneyuki, S.; Sasaki, S.; Nishihara, H. Interfacial Transmetallation Synthesis of Platinadithiolene Nanosheet as a Potential 2D Topological Insulator. *Chem. Sci.* **2019**, *10*, 5218−5225.
(61) Huang, X.; Zhang, S.; Liu, L.; Yu, L.; Chen, G.; Xu, W.; Zhu, D. Superconductivity in a Copper(II)-Based Coordination Polymer with Perfect Kagome Structure. *Angew. Chem., Int. Ed.* **2018**, *57*, 146−150.
(62) Foster, M. E.; Sohlberg, K.; Allendorf, M. D.; Talin, A. A. Unraveling the Semiconducting/Metallic Discrepancy in Ni_3(HITP)$_2$. *J. Phys. Chem. Lett.* **2018**, *9*, 481−486.
(63) Chen, S.; Dai, J.; Zeng, X. C. Metal-organic Kagome lattices M_3(2,3,6,7,10,11-hexaiminotriphenylene)$_2$ (M = Ni and Cu): from semiconducting to metallic by metal substitution. *Phys. Chem. Chem. Phys.* **2015**, *17*, 5954−5958.
(64) Foster, M. E.; Sohlberg, K.; Spataru, C. D.; Allendorf, M. D. Proposed Modification of the Graphene Analogue Ni_3(HITP)$_2$ To Yield a Semiconducting Material. *J. Phys. Chem. C* **2016**, *120*, 15001−15008.
(65) Li, S.; Lü, T.-Y.; Zheng, J.-C.; Yang, S.-W.; Wang, J.-S.; Wu, G. Origin of metallicity in 2D multilayer nickel bis(dithiolene) sheets. *2D Mater.* **2018**, *5*, 035027.
(66) Sproules, S.; Wieghardt, K. Dithiolene radicals: Sulfur K-edge X-ray absorption spectroscopy and Harry's intuition. *Coord. Chem. Rev.* **2011**, *255*, 837−860.
(67) Sproules, S.; Wieghardt, K. o-Dithiolene and o-aminothiolate chemistry of iron: Synthesis, structure and reactivity. *Coord. Chem. Rev.* **2010**, *254*, 1358−1382.
(68) Eisenberg, R.; Gray, H. B. Noninnocence in Metal Complexes: A Dithiolene Dawn. *Inorg. Chem.* **2011**, *50*, 9741−9751.
(69) Clough, A. J.; Yoo, J. W.; Mecklenburg, M. H.; Marinescu, S. C. Two-Dimensional Metal−Organic Surfaces for Efficient Hydrogen Evolution from Water. *J. Am. Chem. Soc.* **2015**, *137*, 118−121.
(70) Grosvenor, A. P.; Kobe, B. A.; Biesinger, M. C.; McIntyre, N. S. Investigation of multiplet splitting of Fe 2p XPS spectra and bonding in iron compounds. *Surf. Interface Anal.* **2004**, *36*, 1564−1574.
(71) Fantauzzi, M.; Elsener, B.; Atzei, D.; Rigoldi, A.; Rossi, A. Exploiting XPS for the identification of sulfides and polysulfides. *RSC Adv.* **2015**, *5*, 75953−75963.
(72) Castner, D. G.; Hinds, K.; Grainger, D. W. X-ray Photoelectron Spectroscopy Sulfur 2p Study of Organic Thiol and Disulfide Binding Interactions with Gold Surfaces. *Langmuir* **1996**, *12*, 5083−5086.
(73) Castillo, O.; Delgado, E.; Gomez-Garcia, C. J.; Hernandez, D.; Hernandez, E.; Herrasti, P.; Martin, A.; Zamora, F. i. Comparative Studies of Oxidation Processes on Group 10 Metals Dithiolene Derivatives in the Formation of Coordination Polymers. *Cryst. Growth Des.* **2018**, *18*, 2486−2494.
(74) D'Alessandro, D. M.; Kanga, J. R. R.; Caddy, J. S. Towards Conducting Metal-Organic Frameworks. *Aust. J. Chem.* **2011**, *64*, 718−722.
(75) Aubrey, M. L.; Wiers, B. M.; Andrews, S. C.; Sakurai, T.; Reyes-Lillo, S. E.; Hamed, S. M.; Yu, C.-J.; Darago, L. E.; Mason, J. A.; Baeg, J.-O.; Grandjean, F.; Long, G. J.; Seki, S.; Neaton, J. B.; Yang, P.; Long, J. R. Electron delocalization and charge mobility as a function of reduction in a metal−organic framework. *Nat. Mater.* **2018**, *17*, 625−632.

DOI: 10.1021/jacs.9b06898
J. Am. Chem. Soc. 2019, 141, 16323−16330